EUROFUSION WPDTT2-PR(16) 16396

M Valisa et al.

Diagnostics, Data Acquisition and Control of the DTT experiment

Preprint of Paper to be submitted for publication in
Fusion Engineering and Design

This work has been carried out within the framework of the EUROfusion Consortium and has received funding from the Euratom research and training programme 2014-2018 under grant agreement No 633053. The views and opinions expressed herein do not necessarily reflect those of the European Commission.

Diagnostics, Data Acquisition and Control of the DTT experiment

R Albanese[1] M Ariola[1] G De Tommasi[2] A Pironti[1] M Cavinato[2] P Fabio[2] A Neto[2] F Sartori[2] R Ranz[2] L Carraro[3] A Canton[3] R Cavazzana[3] A Fassina[3] P Franz[3] P Innocente[3] A Luchetta[3] G Manduchi[3] L Marrelli[3] E Martines[3] S Peruzzo[3] M E Puiatti[3] P Scarin[3] G Spizzo[3] M Spolaore[3] M Valisa[3] G Gorini[4] M Nocente[4] C Sozzi[4] M L Apicella[5] G L. Gabellieri[5], Maddaluno[5] G Ramogida[5]
[1] CREATE, Università di Napoli "Federico II
[2] Consorzio RFX , Padova
[3]ENEA Frascati,
[4]IFP CNR Milano

Corresponding author: Valisa@igi.cnr.it

1. Introduction

The specific mission of DTT [1] will be to explore viable solutions to the power exhaust issues in a fusion reactor in view of DEMO. The ultimate goal will be to qualify and control in various divertor configurations the heat fluxes through the plasma edge in a way that preserves both the integrity of the plasma facing components and the quality of the plasma performance. In this paper we describe the initial approach to the system of diagnostics, data acquisition and control infrastructure foreseen on DTT. The idea behind this approach is that the system of sensors, actuators, models and communication infrastructures must be conceived in an integrated way. This is mandatory in order to assure that the many interlaced functions of a complex fusion device, such as plasma control, machine-protection and safety, are fulfilled simultaneously. In the second place, whereby some redundancy is foreseen for model validation and reliable feedback control purposes it is important to bear in mind that one of the ultimate goals of DTT will be to explore DEMO relevant ways to control complex situations, that is with a minimal amount of direct measurements of the plasma parameters. This is to be accomplished by relying more and more on physics and engineering models driven controls [2].
The compatibility of the diagnostics with the present machine design has been verified particularly with regard to the geometry and paying attention to several other important specifications such as electromagnetic and radiation compatibility as well as maintenance issues. However an exhaustive verification of all these aspects is beyond the scope of this work.

In Chapter 2 the diagnostics system is described, mainly in terms of their functionalities and their main specifications. A set of fundamental diagnostic has been selected for both the development of the scientific basis of the experiment, the protection of the machine and the stable operation of the discharge under robust real time control. Chapter 3 describes in more details some of the principal situations where feedback control will be necessary for assuring long pulses, with particular reference to the specific mission of DTT. Data acquisition and control system that have been conceived according to modern schemes and tools are illustrated in Chapter 4 before some final remarks.

2. The DTT Diagnostics

The main DTT diagnostics so far conceived for DTT are listed in Table 1 according to the parameters to be measured. Soon after a brief description is given of the most relevant diagnostic systems.

Magnetic diagnostic

The magnetic diagnostics are relevant to all of the basic functions (machine protection, plasma control, physics studies and performance evaluation). Sub-systems may be conceived on the basis of the different measurement techniques: Magnetic flux sensors; Magnetic field probes; Current transducers. Several plasma parameters can be deduced by a combination of different magnetic sub-systems, which can have therefore different roles in the architecture of the magnetic diagnostic (primary, backup, supplemental).

Table 1 *Main DTT diagnostics*

Paramete	***Diagnostic***	***Characteristics***	***Resolution***	***Parameter***	***Diagnostic***	***Characteristics***	***Resolution***
Te Core	Thomson Scattering	Fibre optic I.Filters polychromators	10 cm, 10 ms	Ne Core	Thomson Scattering	Internal optics required.	10 cm, 10 ms
	ECE : O1 covers the full radial profile, X2 covers the LFS up to the center	O mode (O1: 130<f<250 GHZ) and 2nd harmonics, X mode (X2: 260<f<380) detectable	1-2 cm FW @ 1/e , 0.1 ms	Real Time Ne Core	MIR Interferometer / FIR Polarimeter Vibraton compensated.	Few chords MIR , high resolution FIR Internal optics, QCL lasers	0.1 ms, 1cm - 10cm
Ti	Crystal Spectrometer	Ar XVII & Ar XVIII for Te< 5 keV, Kr XXV otherwise	20 cm, 10 ms	Neutrons yield	Fission Chambers		10 ms
	Charge Exchange	Diagnostic Beam	50 ms	Neutron emission profile	Camera/ Scintillators & Diamond det.	from low to high neutron yield (1.3·1017 n/s).	10 ms
Ion Flow Plasma Core	Crystal Spectrometer & CHRS	Geometry	20 cm, 10 ms	Fast ions & Runaway electrons	TOF & LaBr3 γ detector camera	Neutron and γ cameras can be integrated	10 ms /0.1ms
Currents	Rogowski coils, Resistive Shunts		0.1 ms		Visible Survey spectrometers	Imaging mode	2 mm in imaging mode
Magnetic Flux	Flux Saddle and diamagnetic Loop		0.1 ms	Divertor Te	Thomson Scattering	Standard	< 1 cm, 10 ms
Magnetic Field	Pick up coils, Hall Probes Polarimeter	MIC, LTCC technology	0.1 ms	Compression Enrichment	Spectroscopy	Ar, He Lines ratio	1 cm , <10 ms
Plasma position and shape	Flux and Saddle Loops and magnetic field probes		0.1 ms		Langmuirprobes		1 cm, 1 ms
Plasma position and shape	Inner and outer reflectometer channels	Inner antenna layout	0.1 ms		Penning gauge spectroscopy	Magnetic Field screened	10 ms
	CCD imaging	Interference filters	10-20 ms	Neutrals (pressure)	Fast Baratron		ms
Plasma Energy	Diamagnetic loops		0.1 ms		RGA		100ms
q profile	MSE		10 cm , 10 ms		Filtered CCD cameras		10 ms, 2 mm
q profile	FIR Polarimeter	multichord	0.01 ms	Wall loading temperature	NPA	Energy lower limit	5 ms
MHD	Magnetic Field probes		0.1 ms		High resolution Spectr.		10 ms
MHD	ECE		0.1 ms		IR camera	Impact of redeposition layers	ms
	SXR tomography		0.1 ms				
Radiation	Bolometer array	Metal foil /AXUV	2 cm, ms		instrumented tiles	Thermocouples, Langmuir probes	ms

	SXR diodes array		3cm, 0.1 ms	Runaway electrons	HXR / γ-Rays		
Zeff	Interference filters 5235.5 A and	Tangential chords and viewing dumps	0.1 ms		Visible Cameras	Co- and counter current views	10 ms
Zeff	Low resolution spectrometer	Tangential chords and viewing dumps	10 ms	Halo/Hiro Currents	Halo sensors		ms
	Crystal Spectrometer		10 ms	Vessel deformation	Strain Sensors/optical sensors		
Impurities Core	VUV Survey spectrometer		10 ms	Redeposition layers	LIBS		
	SXR tomography	Si detectors,	5 cm, kHz		Microbalance	Environment compatibility	100 ms
	Laser Blow Off	Target layers	multipulse	Wall Hot Spots	CCD monitor	Pattern recognition	1 mm
	VUV/VIS/NIR spectrometers	Ionization, Balmer & Paschen series	10 ms, > 1 cm	Escaping Fast ion	Scintillator probes		1 ms
Divertor detatchment	Retarding Field analyzer		1 ms		Faraday cups		1 ms
	Heterodyne Doppler		3mm				
	Filtered CCD	3Dimaging software development	2 mm , 10 ms				

Exhaustive literature about generic magnetic diagnostics can be found in [3] but in general the DTT design inspires to the specific design of ITER [4]. The actual layout of the magnetic diagnostic for DTT will be defined once the main DTT components are refined (in particular Vacuum Vessel, First Wall and Divertor).A very preliminary estimate of the total number of magnetic sensors for DTT is expected to be of the order of one thousand (in between the number of sensors presently exploited at JET [5] and foreseen for ITER [6], that is approximately 500 and 1500 respectively).The design and manufacturing of magnetic sensors for DTT could also benefit from recent developments for ITER [7, 8], such as loops and windings made of Mineral Insulated Cables and magnetic field probes based on LTCC technology (Low-Temperature Co-fired Ceramics) with pickup coils more compact and less sensitive to detrimental radiation induced effects.

Neutron, gamma and Hard X-ray diagnostics

Given the high neutron yield of 1.3×10^{17} n/s expected in DTT a set of neutron counters [9], a neutron/γ-ray camera and high resolution neutron and gamma-ray spectrometers are deemed suitable to measure the neutron yield, the profile of neutron emission and the supra-thermal components (accelerated fuel or ^{3}He ion population) respectively. A time of flight instrument along a dedicated line of sight and with the improved design deployed at EAST [10] would provide the adequate sensitivity (10^{-4} of the main thermal neutron emission) to study energetic tails [11, 12]. High efficiency liquid scintillator and less sensitive but robust single crystal diamond [13] for neutrons and high purity germanium detector or $LaBr_3$ scintillators [14] would o cover the whole dynamic range of neutron emission expected in DTT operations. Measurements of γ -ray emission generated from reactions between the energetic ions and impurities [15, 16] will be carried out. The γ -ray and neutron cameras can be integrated like in JET. γ -ray detectors can be used also to measure the profile and spectrum of hard x-ray emission from runaway electrons.

ECE radiometer

Suitable for electron temperature measurements, MHD detection, kinetic profile analysis and pedestal characterization, preliminary evaluations of the ECE radiation as detected by an antenna located at R=3. 25 m, z=0.15 m and radial line of sight have been performed. Both 1st harmonics, O mode (O1: 130<f<250 GHZ) and 2nd harmonics, X mode (X2: 260<f<380) spectral regions are detectable with adequate radial resolution, of the order of 1 cm for

the X2 and 2 cm for O1, respectively. The X2 has appropriate resolution for spatial detection of the MHD activity. O1 measurements in the HFS might be used for the characterization of the kinetic quantities in the pedestal.

Interferometer-polarimeter

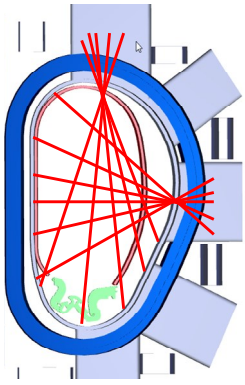

Figure 1: interferometer-polarimeter viewing chords.

Two interferometer-polarimeter systems are foreseen: a few channels mid infrared (MIR) 10. 5 μm CO2/CO *toroidal* systems and a higher spatial resolution *poloidal* far infrared (FIR) one. The MIR vibration compensation scheme successful in both FTU and RFX-mod devices provides the reliable real time measurement of the chord averaged electron density. The multichord FIR system measures the density and the plasma current profile (see Fig.1). In the low/medium density cases the FIR system will provide a good magnetic field measurement and the MIR one will provide vibration compensation for density measurement, while in the high density case the short wavelength alone can provide magnetic field measurement from faraday rotation and density measurement from the Cotton-Mouton effect. Optimal laser source solution for polarimetric measurements resilient to density gradients is the 100/50 μm one. Optically pumped CH3OH 118 μm gas lasers are commercially available (e.g at RFX-mod). Gas laser sources in the 50 μm range are yet unavailable but the so called theraHz domain of QCL lasers is progressing. A conservative solution would be to use a 10. 6 μm CO2 laser for the vibration compensation..

Charge Exchange Spectroscopy

The most common diagnostic to measure the ion temperature and the collective flow is Charge eXchange Recombination Spectroscopy.

In absence of a suitable heating beam a diagnostic beam is to be considered. Simulations show that a beam of more than 80 keV and of several A of equivalent current are required to obtain sufficient active signal. The presence of W in the plasma facing components adds the extra complexity of a rich background spectrum.

Crystal Spectrometer

An alternative system to measure the ion temperature is the X-ray crystal spectrometer. The imaging detector can be well screened from harsh radiation as it does not look directly at the plasma. Large detectors (100 x 300 mm) have been developed for KSTAR, NSTX and EAST and will be used on ITER. The issue of wavelength calibration has been solved on C-mod in discharges with non-rotating plasma. The spatial resolution is determined by detectors (for C-mod pixel size 0. 172 x 0. 172 mm) and by the distance between plasma and crystal (for EAST < 1 m).

Bolometry

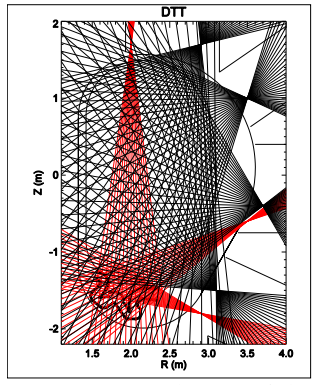

Figure 2, Distribution of the bolometer arrays

Real-time bolometry is to be used to optimize the divertor power exhaust. Bolometric detectors based on metal foil are typically used and radiation hard versions have been developed for ITER**Errore. L'origine riferimento non è stata trovata.** Faster and compact detector, based on Silicon photodiodes AXUV has been tested on ASDEX and on C-mod even though its spectral sensitivity is not uniform in the VUV range and its performance a degrades strongly over time. A state of the art bolometric diagnostic is installed in ASDEX with 112 foil detectors and 256 AXUV detectors0 The foil based tomography in DTT could rely on 3 main heads hosting three fans covering the plasma core and 3 additional heads directed towards the divertor as indicated in **Fig. 2**.

Soft X-Ray radiation

Soft x-ray tomography is a powerful tool to diagnose both impurities accumulation in the core and MHD activity in the hot plasma core, such as ELMs, sawtooth activity, or Fast Particles induced instabilities, e.g. Toroidal Alfven Eigenmodes.

Typical state of the art SXR diagnostic, designed for shaped plasmas have been installed in JET and in ASDEX . In ASDEX 8 pinhole cameras are installed with about 200 lines of sight. Silicon diodes are used, screened by a curved Be filter 75 um thick. Required bandwidth is 1MHz, in order to detect also high frequency MHD.

Charge exchange neutrals

Neutral particles play an important role at the edge of the plasma and in the divertor region. Low energy escaping neutral particles can be detected by a time of flight neutral particle analyzer with an adequately long path. The energy distribution information can be complemented by the analysis of the shape of the D alpha emission line as detected by a high resolution spectrometer. Coupling energy and density information yields the neutral pressure in the observed region.

Divertor Thomson Scattering

Besides a core Thomson Scattering, a standard Thomson Scattering layout is specifically foreseen for th edivertor, with fiber optics defining the scattered volume and interferential filter polychromators to analyse the signal. The main purpose is to detect a detachment states. A preliminary design maximizing solid angles, laser alignment reliability, minimizing stray light, optimizating spectral channel ranges, detectors and amplifiers seems to fit the requirements for the 1-10 eV Te range measurement, with densities around $1x10^{19}$ m^{-3}. Assuming efficiency values typical of the Thomson Scattering system of RFX-Mod, sufficient signal is expected. **In Errore. L'origine riferimento non è stata trovata.** red dots show the proposed scattering volumes with sub centimeter resolution. Laser relays and collection optics share the same mechanical support improving alignment reliability. Improvements of the layout, with multiple laser passages and laser dump outside the vessel are being considered that would imply changes in the ports designs.

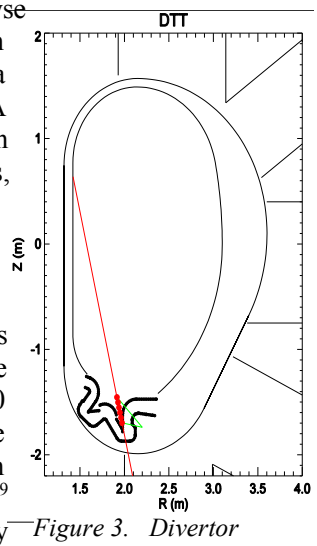

Figure 3. Divertor Thomson Scattering Layout

Zeff

The measurement of the effective charge Zeff is based on the continuum radiation in the standard 523. 5 nm region collected by means of interference filters, 1 nm of bandwidth, and photomultipliers as the detector. Contamination is possible from several elements such as: Ne, Ar, Xe, Mo, W, Fe. In such cases spectrally resolved survey between 350 and 900 nm, whereby the continuum is expected to display its $1/\lambda^2$ dependence, may be of help. Observations along the toroidal direction are less affected by edge contamination and light reflection issues.

Divertor Spectroscopy

Emission spectroscopy is a multiopurpose tool in the divertor plasma. T_e and n_e can be inferred from line intensity ratios Dα tomography can be achieved by means of arrays of LOS from the upper port and a couple of arrays from the side, through interspaces between divertor modules. Feasibility of LOS directly aiming at tiles is to be pursued. Balmer or Paschen series are a good monitor of the recombining status of the plasma CCD images can monitor the ionization front. These systems can be used for real time control of detached regimes. For the flow profile Mach probes and emission spectroscopy are used.
In DIIID for divertor flow imaging also a heterodyne Doppler "coherent imaging" system is used, where a tangential real image is transferred to a polarization interferometer, equipped with a camera detector. Time resolved 2D images of integrated line brightness, velocity, ion temperature. tomographic unfolding of flow and temperature can then be obtained [18].

Divertor and SOL probes

Insertable probes determine local kinetic parameters and turbulence microstructures. Both inner and outer divertor components will be equipped with Langmuir probes to detect particle fluxes, electron temperature and electron density and plasma flow. Retarding field analyzers will be used instead to characterize the ion temperature. Additionally a set of embedded treble coils to measure the electromagnetic radiation and its mode spectrum will allow the study of the discrete events that characterise the edge palsma, particularly during ELM events.

Plasma Wall Interaction monitoring system

The wall and the divertor will be monitored by a set of visible cameras and Infrared cameras. Visible cameras are meant to serve as general monitor system during the discharge in particular with recognition capability of hot spots or abnormal events, but will be used also as detectors for real time control of the detachment phase and of the plasma position as a DEMO relevant alternative to magnetic probes or thermocouples IR cameras will be installed to monitor surface temperature of PFC.

Fast Ion losses

Fast ion detection is important to establish the contribution of this components of the escaping particles to the overall power exhaust. Diagnostics for the purpose will rely on gamma ray detection and on edge scintillator probes

In situ PFC analysis

To monitor the surface layer composition and the fuel gas content of the plasma facing components the well established tool of Laser Induced Background Spectroscopy (LIBS) represents an ideal candidate with remote analysis capability and microdestructive characteristics. The feasibility of in-situ LIBS diagnostic of surface layer composition was demonstrated on FTU [17].

3. Real Time Control

Active feedback control of the plasma state represents a key element for stationary tokamak operation and will become even more important in future reactors.. Plasma current, density, equilibrium, Beta, MHD control (NTM, RWM, ELMs frequency and amplitude), power exhaust control are some of the areas where feedback is to be applied. As an example the following section introduces a state-space linear model that describes the behaviour of the plasma column and of the surrounding active an passive conductive structures, around a given MH equilibrium and that will be exploited to design the proposed plasma magnetic axisymmetric control system for DTT and to estimate the power required to stabilize and control the plasma. *Engineering-oriented* models enable model-based design of control systems. Simpler than *physics-oriented* simulation codes, such as transport codes [2, 19, 20], such linear models permit also to automate both the validation and deployment of the plasma axisymmetric magnetic control [21, 22, 23, 2] but are also used to support the design and commissioning of the plasma magnetic diagnostic [24], as well as to run inter-shot simulations aimed at optimising the controller parameters

.

Table 2 . Main objectives of feedback control

	Diagnostics	**Actuators**	**Control scheme**
Plasma Current	Rogowsky Coils	Magnetic Flux	PID
Axisymmetric equilibrium	Pick up coils /loops	PF coils	PID; Physics Model
Electron Density	Interferometer/polarimeter	Gas valves/ Criopumps	PID
MHD / NTM,RWM	Pick-up coil, ECE ($\Delta\rho \leq 0.1$), SXR	ECE/Control Coils	PID; Physics Model
MHD / ELM control	Dα, Stored energy	Control Coils, Plasma shape, Vertical kicks, Pellets / RMP's	PID; PhysicsModel
Plasma Detachment	IR Cameras / thermocouples / CCD cameras /spectroscopy /Thomson Scattering	Fast gas valves for D2 and impurities (placed near the strike points);	PID; Physics model
Radiation/ Enrichment factors	Bolometer arrays, SXR arrays and VUV spectrometers for the core radiation; Bolometer cameras, spectrometers in the divertor region;	far-away valve acting on the core density	Feedback control system (PID)
Divertor Heat Flux	Infrared cameras Langmuir probes and thermocouples embedded in the divertor plates Thomson scattering High speed cameras equipped with suitable interference filters. Magnetic measurements	in-vessel coils; Plasma Shaping and position; ECRH for heating	

3.1 Plasma modeling for magnetic axisymmetric control

The proposed linearized plasma/circuits model can be specified as the state-space model [25]

$$\delta\dot{x}(t) = \mathbf{A}\delta x(t) + \mathbf{B}\delta u(t) \quad (1a)$$

$$\delta y(t) = \mathbf{C}\delta x(t) + \mathbf{D}\delta u(t) \quad (1b)$$

with the state vector given by

$$\boldsymbol{\delta x} = \begin{pmatrix} \boldsymbol{\delta I_{PF}} \\ \boldsymbol{\delta I_{IC}} \\ \boldsymbol{\delta I_p} \\ \boldsymbol{\delta I_E} \end{pmatrix} \textbf{ and } \boldsymbol{\delta x} = \begin{pmatrix} \boldsymbol{\delta U_{PF}} \\ \boldsymbol{\delta U_{IC}} \\ \boldsymbol{U_p} \\ \boldsymbol{\delta WI_p} \\ \boldsymbol{\delta \dot{WI}_p} \end{pmatrix},$$

where:

- **A**,**B**,**C** and **D** are the model matrices;
- $\delta I_{PF} \in \mathbb{R}^{n_{pf}}$ is the vector of the current variations in the active superconductive PF circuits, which are placed outside the vessel; together with ones in the in-vessel coils, these variations represent the control *knobs* for plasma magnetic control;
- $\delta I_{IC} \in \mathbb{R}^{n_{ic}}$ is the vector of the current variations in the active in-vessel circuits;
- $\delta I_p \in \mathbb{R}$ is the plasma current variation;
- $\delta I_E \in \mathbb{R}^{n_e}$ is the vector of the eddy current variations in the passive structures;
- $\delta U_{PF} \in \mathbb{R}^{n_{pf}}$ is the vector of the input voltage variations applied to the PF circuits;
- $\delta U_{IC} \in \mathbb{R}^{n_{ic}}$ is the vector of the input voltage variations applied to the in-vessel circuits;
- $U_p = -r_p I_{p_0}$ is the opposite of the equilibrium plasma voltage;
- $\delta WI_p \in \mathbb{R}^{n_d}$ is the disturbances vector, where $WI_p = \left(\beta_p I_p \;\; l_i I_p\right)^T$, where β_p is the poloidal beta, and l_i is the plasma internal inductance1;
- $\delta y \in \mathbb{R}^{n_y}$ is the output vector, that includes all the variables that need to be controlled (e.g., the plasma current I_p, the currents in the PF circuits, the plasma vertical position and the descriptors of the plasma boundary). Linear models in the form are automatically generated around a given equilibrium by the CREATE 2D nonlinear equilibrium codes [26, 27] in the Matlab/Simulink environment. These equilibrium codes and the corresponding linearized systems have been extensively validated against different fusion devices such as RFX [28], JET [29] and the EAST tokamak [30]. The same modelling tools are currently used also to perform preliminary studies and code benchmarking for both ITER [31] and DEMO [32]. Incidentally, the CREATE-NL+ equilibrium code [27] can be integrated with a transport solver [33]. The availability of two different equilibrium codes, hence of two different ways to generate linearized models, is relevant for code benchmarking and to increase the reliability of the overall model-based design environment.

1 The variations of β_p, l_i and the plasma current itself are seen as disturbances from the point of view of the overall magnetic control system.

3.2 Model-based magnetic axisymmetric control

Before estimating the performance of the vertical stabilization system by means of the linear model a preliminary architecture for the DTT magnetic control system is proposed. Then, the best achievable performance in rejecting VDEs, ELMs and H-L transitions will be presented.

3.2.1 Architecture of the plasma axisymmetric magnetic control system

A block diagram of the overall magnetic control system architecture is reported in Fig. 4:

- a *PF Current Decoupling Controller* guarantees that the currents in the PF circuits track the *scenario* references *currents* (feedforward action) requested by the outer control loops. The closed-loop bandwidth for the PF Current Decoupling Controller is mainly limited by the voltage limits of the power supplies and by the presence of the passive structures.
- a *Plasma Vertical Stabilization Controller* stabilizes the vertically elongated and unstable plasma column by exploiting the in-vessel coils; The Vertical Stabilization Controller has in input the vertical velocity of the plasma centroid and the current flowing in the *C*5−*C*6 in-vessel coils pair, and generates as output the voltage references for these two copper coils. If needed, in order to avoid current saturation in the in-vessel coils the superconductive PF coils can also used as actuators for vertical stabilization [34]
- a *Plasma Current Controller* tracks the reference plasma current by driving a set PF current deviations (with respect to the nominal values), which are proportional to a set of currents providing (in the absence of eddy currents) a *transformer field* inside the vacuum vessel, so as to reduce the coupling with the Plasma Shape Controller. In this architecture, the Plasma Current Controller is based on a simple proportional-integral-derivative (PID) controller.
- a *Plasma Shape Controller* tracks a set of plasma shape descriptors and generates PF current deviation references to the PF Current Decoupling

Controller. The plasma shape descriptors are usually computed by a plasma boundary reconstruction code, it computes a set of PF current. In the proposed architecture, an eXtreme Shape Control *XSC-like* approach is considered [35]. This approach has been proven effective to control high elongated plasma shapes both directly controlling the plasma-wall gaps [36] or by performing isoflux control [37]. By using an XSC approach it is possible to easily include current limit avoidance algorithms [38]. Furthermore, with the XSC it is possible to control simultaneously the plasma boundary and the flux expansion, and hence the heat load on the divertor, as it has been proposed for the EAST tokamak in [37]

3.2.2 Best achievable performance of the vertical stabilization system

Given the maximum values for the voltage and absolute current of the four quadrants power supplies for the the *C5−C6* in-vessel coils (200 V 25 KA, 100 kAper turns) [39], the model presented in Section 3.1 has been exploited to estimate the best achievable performance for the plasma vertical stabilization controller.First of all, the maximum rejectable VDE has been evaluated for a set of four different plasma equilibria. The results are summarised in Table 3, where, for each of the considered equilibria, the maximum rejectable VDE is reported together with the time t_{stop} needed to invert the plasma velocity[2]. It can be noticed that the maximum VDE is about 10 cm, while t_{stop} is always less than 10 ms. The performance of the vertical stabilization system has been further assessed by considering the response to a 1.2 MJ ELM at high β_p. Such an ELM has been modeled as a poloidal beta drop

$$\Delta\beta_p = -\frac{8\Delta W_{DIA}}{3\mu_0 I_p^2} \cong -0.033,$$

and an increase of the internal inductance l_i given by $\Delta l_i = -\Delta\beta_p = 0.033$. By exploiting again the linear model , an equivalent VDE has been computed for the considered ELM, together with the correspondent t_{stop}. The results are reported in Table 4, where it is shown that in this case the most challenging equilibria is the one corresponding to

Table 3: Maximum rejectable VDE when the IC5−IC6 pair is used to stabilize the plasma. The coil pair is assumed to be fed in anti-series with V_max=200 V and I_max=25 kA

Equilibrium	equivalent VDE $[cm]$	t_{stop} $[ms]$
SN @42 s (high β_p)	~2	~5.1
QSF @ EOF	~3	~7.3
SF @ 42 s	~7	~15.6

the snow-flake configuration. Eventually, similarly to what has been done for the 1.2 MJ ELM, the.

behaviour of the vertical stabilization system has been checked also against an H-L transition, which has been identified as a poloidal beta drop $\Delta\beta_p = -0.37$, and a drop of l_i of $\Delta l_i = -0.02$. The results are reported in Table 5, where the maximum inboard displacement is also given. In this case the vertical stabilization system shows good performance regardless of the considered equilibria. Moreover, it should be noticed that the inboard displacement would be further mitigated by the plasma shape controller.

Equilibrium	growth rate γ $[s^{-1}]$	maximum VDE $[cm]$	t_{stop} $[ms]$
SN @32 s (low β_p)	~20.7	~10	~7.6
SN @42 s (high β_p)	~19.8	~12	~9.1
QSF @ EOF	~34.1	~11	~8.2
SF @ 42 s	~80.2	~9	~9.8

Table 4: Equivalent VDE and t_{stop} for a 1.2 MJ ELM. A vertical stabilization control system that uses the IC5−IC6 pair is considered. The coil pair is assumed to be fed in anti-series with $V_{max} = 200\,V$ and $I_{max} = 25\,kA$.

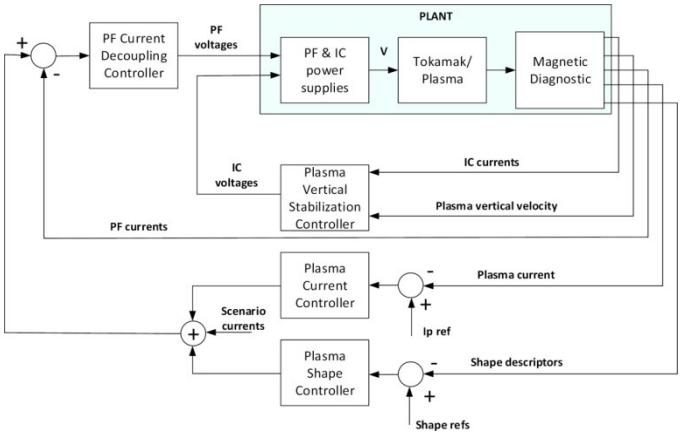

Figure 4: Main blocks of the DTT magnetic control system architecture. The currents scenario represent the nominal PF current references designed offline and that are to be tracked by the PF Decoupling Controller, in order to obtain the desired plasma scenarios

2 From the vertical stabilization point of view, a VDE is equivalent to a sudden and almost instantaneous change in plasma vertical position and velocity. It turns out that a VDE can be conveniently modeled as instantaneous change of the state in the linear model

Equilibrium	uivalent VDE $[cm]$	maximum inboard lisplacement $[cm]$
SN @42 s (high β_p)	~1	~1
QSF @ EOF	~1	~1
SF @ 42 s	~2	~1

Table 5: Equivalent VDE and t_{stop} for an H-L transition. A vertical stabilization control system that uses the IC5−IC6 pair is considered. The coil pair is assumedto be fed as in Table 4.

3.3 Power Exhaust Control

In the context of the the exhaust control on DTT, the scenario of partially or completely detached plasma is of particular interst. Core radiation will be monitored by a series of bolometer arrays, SXR arrays and VUV spectrometers, while in the divertor region three additional bolometer cameras are considered to enhance the local resolution capability to the cm level. The radiation diagnostics of the divertor are complemented spectrometers ranging from VUV to NIR wavelength. Balmer and Paschen series are indeed suitable to monitor the recombination process that occurs in the detachment phase, as demonstrated on C-Mod [40] and NSTX [41,42] while visible spectrometers measure the impurity influxes, which also decrease in the detachment phase. High speed cameras equipped with suitable interference filters can be used for real time optical plasma boundary reconstruction as shown on TCV [43]. Recently developed codes such as OFIT, allow for a fast, non-iterative analysis of the spectrally resolved images with low latency, to identify radiative shell edges in the image-emissivity [44]. In particular plasma boundary reconstructions of diverted plasma discharges have been obtained, showing agreement of within 1 cm with magnetic equilibrium reconstruction. Infrared cameras detect the heat flux profiles at inner and outer strike points. The set of diagnostics is complemented by Langmuir probes and thermocouples embedded in the divertor plates, which monitor particle and energy fluxes, a spatially resolved (several millimeters) electron temperature profile measurements (Thomson Scattering) in the range 1-10 eV and by pressure gauges in the regions where pumps are located. The temperature measurements together with the magnetic measurements will be used by a feedback control algorithm acting on the currents in the in-vessel coils for the realization of the plasma advanced magnetic configurations (e.g. wobbling, strike point sweeping, etc.) and, more in general, for the control of the plasma strike point position and flux expansion. Regarding the possibility of having a detached regime in DTT, the main actuators are the fast gas valves for D2 and impurities placed near the strike points acting together with a far-away valve, which keeps the core density stationary. A fast heating system such as ECRH should compensate for overshoots of the radiative power.

The feedback loop for detachment control keeps the ionization front at a specified distance from the plates by regulating gas injection, based on the electron temperature profile measurements and/ or other information from bolometry, cameras and spectroscopy, while the core density is maintained constant by a different loop. Bolometry is used to detect the possible formation of localized radiation condensation (MARFE's [45]). A similar technique has been demonstrated on DIII-D [46].

In addition, impurity accumulation in the ore can be contained by ICRH and ECRH due to a variety of mechanisms – fast ion effects enhancing neoclassical screening , electron to ion heat flow ratio maximizing the turbulent transport [47]

Feedback systems will be firstly based on standard PID control. These systems have proven to be successful for example in DIII-D to control the detachment position.

Morover, inclusion of the real-time plasma shape measurement by means of fast cameras described above in a feedback control loop for the plasma position, has demonstrated effective stabilization of the plasma vertical position. A real time analysis method for the plasma periphery has been demonstrated at 1kHz with two cameras [48]. Ideally, a collisional-radiative model could calculate the emission for the different ionization stages and spectral transitions based on previous impurity density and local temperatures and the knowledge of the plasma composition and flag the proximity to operational limits or actuator constraints. To our knowledge however the first principle physics codes cannot yet predict the transition from attached to detached , and this represent an area of possible development.

3.4 MHD Control

A provisional set up for NTM and ST control by means of the 170 GHz ECRH launching has been conceived by means of the GRAY code (ECRH&ECCD) [56] and with the SPECE code (ECE) [57]. The system is based on 4 poloidally steerable 1 MW beams located in the upper port to minimize trapped electrons effects preserving the access to the HFS with Real Time capabilities. A toroidal steering of around 10-15 degrees is still to be considered. Several hardware specifications have been defined: cooling requirements, antenna concept, diamond window , focussing optics, plug-in supporting structure. Optimized current drive efficiency at accessible radial ranges is obtained from the Upper and at the q=1, 3/2 and 2 surfaces has been estimated to be Icd=9, 3.7 and

2.2 kA/MW respectively. The power and current drive radial localization $\Delta\rho$ along the accessible radial range is $\Delta\rho \leq 0.1$. Which is promising towards NTM stabilization.
As to the Resistive Wall Modes no specific modeling of active mitigation for safety purposes has been carried out yet, which will be important to define the specifications of the internal correction coils.

3.5 ELM Control

Vertical kicks, pellets and Resonant Magnetic Perturbations, have all been successful in some way to pace the ELM in a controlled manner in various experiments. In a different approach the pedestal region is maintained in a state of quasi relaxed situation where no ELM's are generated. The I-mode in C-mod, the Quiescent H Mode and Super H-mode in D-III are such examples, all characterized by the presence of a continuous mode or broadband MHD spectrum. ELM'free plasma's in DIII-D are reached with sufficiently high EXB shear, which can be manipulated by means of the NBI torque and plasma shaping. The torque exerted by non-axisymmetric non-resonant magnetic perturbations has also been successful in reaching the QH mode with zero net NBI torque [58]. Injection of Li, which modifies the edge density profile has also lead to ELM free regimes in DIIID. Modelling of DTT scenarios is required to estabilish which technique is the most appropriate to stabilize ELM's, depending also on the systems available for the purpose. The use of internal coils for RMP production is in fact still under discussion.

4. DTT Instrumentation & Control System DICS

A brief survey of the main preliminary choices made to integrate tools and control system of DTT is given below.

Main Functions

A modern fusion device is a large and complex civil and mechanical construction surrounded by a number of industrial plants which are meant to supply the necessary fuelling, power, and cooling to the tokamak load assembly standing at the centre of it all. Essential both for the operation of each component and for the coordination of the ensemble, is the Instrumentation & Control System (I&C). It consists of all the sensors, actuators, controllers, and man machine interfaces necessary for the systems to perform their duties according to the user needs. I&C is specified in term of the functionalities (functions) that it provides. For good practical and regulatory reasons, functions are divided into the following categories: control, machine-protection and safety. For each category different design and quality requirements are applied both to comply with regulatory prescription and to better focus the engineering costs.
Safety I&C provides functions meant to help reducing any harm risk to people. Machine protection functions aim at reducing the total cost of ownership both by reducing the chance or the consequence of a plant failure and by reducing downtime. Control I&C functions are those necessary to help implement the needed features of the facility.

Architecture

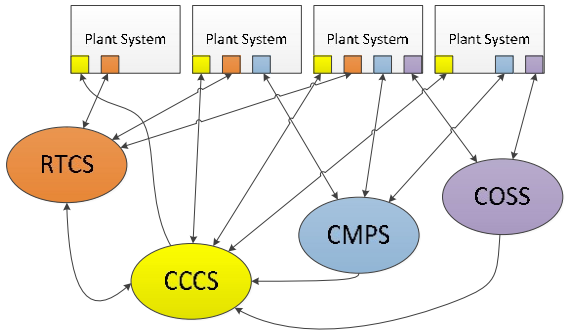

Figure 5 – DICS architecture

Architectural blocks.

DICS architecture design identifies the components of DICS and provides a brief description of the interfaces among components.
The first architectural choice is the division of DICS between central systems and plant systems. Plant System I&C contains sensors and actuators and performs all the functions necessary for the standalone operation of one part of the plant (for example a PF power supply or the electrical distribution). Central I&C Systems are those instead concerned with the coordinated operation of Plant Systems.
The second architectural choice is the division of central DICS into four major systems on the basis of the main categorisation of functions:

- COSS Central Occupational Safety System
- CMPS Central Machine Protection System (hard investment protection functions)
- RTCS Real Time Control System (network of collaborating Systems)
- CCCS Central Command and Control Systems (including data collection and monitoring)

CCCS and RTCS both provide control I&C functions, but are distinct because the former provides functions necessary for the configuration, coordination and activation of systems, while the latter provides functions necessary for the operation of systems.
For large Plant Systems the same subdivision used for the central systems, should also be applied when

it leads to a more rational development, easier to manage and maintain.

Main interfaces

Interfaces may exist between a Plant System and any of the central systems. Interfaces among Plant Systems are provided by the RTCS network. Direct interfaces are possible but should be limited.

For cost and maintenance reasons, one important objective is to design and manufacture Plant Systems using as much as possible industrial standards. For this reason the interfaces between Plant Systems and CCCS will employ as much as possible open industrial standards like OPC open architecture over a dedicated network infrastructure CCCSN. To collect large volumes of experimental data DTT will instead employ a custom distributed TCP based client server system like for instance MDS+[56].

Safety and Machine Protection functions will be implemented as close as possible to the Plant and will be organised around the affected actuator. When measurements from a different plant are needed, the needed sensors will be either shared or transferred functionally to the needing system. Interfaces to the CMPS and COSS will be kept to the minimum and implemented employing the simplest mechanism.

RTCS is a set of collaborating Plant Systems and Systems intercommunicating over a dedicated network RTN. This network will have multi-star topology and employ multicast UDP with a custom application layer. In order to allow qualification of the network, the traffic will be stationary, with the same pattern of packets repeating with a frequency faster than 10Hz. This means that all the transmitters will be synchronised with common central clock and will send data with frequencies multiple of 10Hz. Packet content and multicast circuits will be prescribed centrally.

Control Hierarchy

Figure 5 shows a flat 2 level architecture for DICS where all the plant systems occupy one level and all the central systems the other. In fact Plant Systems will be internally organised hierarchically, possibly with a distinct number of levels for control, investment protection and safety. The specific architecture will be driven by the operational needs, with as many subdivisions as needed independent operations of subsystems during commissioning or maintenance. Safety and machine protection will typically require a more monolithic implementation as segregated protection is only possible if true segregation of the sub-plants is implemented.

Within the central systems also limited hierarchy will be implemented. The main design driver will be the need to allow both coordinated and segregated operation of groups of plant systems (for instance during commissioning).

Preliminary technological choice

For Plant System, a standard industrial solution will be preferred: PLCs and remote IOs interconnected via a field bus (for instance PROFINET). No specific brand of PLC will be selected, but the focus will be on openness and on interoperability.

For all the functions where PLCs are not applicable, the choice will be a solution employing PC Server Machines and remote IO (PCI-express or Ethernet) on adequate chassis (for instance ATCA or compact PCI-express).

Whenever demand for reaction time or computational speed exceeds what the above hardware can provide, solutions based on FPGA or parallel processors (GPUs) will be investigated.

For investment protection and safety, in addition to the above consideration, for the hardware and software tools, qualification to relevant standards will be required.

5. Final remarks.

An overview of the diagnostic and control system conceived so far for DTT has been given. Focussing on the specific mission of the machine, diagnostic and control system will provide the tools to experiment and optimize various solutions for the power exhaust control, involving tailored magnetic topologies highly radiative regimes, advanced materials and with a particular vocation to develop model driven schemes for control in preparation of DEMO.

Acknowledgements

This work has been carried out within the framework of the EUROfusion Consortium and has received funding from the Euratom research and training programme 2014-2018 under grant agreement No 633053. The views and opinions expressed herein do not necessarily reflect those of the European Commission

References

[1] DTT

[2] F. Felici, et al., Development of real-time plasma analysis and control algorithms for the TCV tokamak using Simulink, Fus. Eng. Des. 89 (2014) 165–176.

[3]E. J. Strait, et al, "Magnetic diagnostics", Fusion Science and Technology, 53, 2008, 304-334

[4]Vayakis G. et al., “Development of the ITER magnetic diagnostic set and specification”, Review of Scientific Instruments, 83 (2012) 10D712

[5]JET Magnetic Diagnostics: <http://users.euro-fusion.org/pages/mags/index.html>

[6]D. Testa, et al., “The magnetic diagnostics set for ITER”, IEEE Transactions on Plasma Science 38 (2010), 284-294.

[7]G. Vayakis, et al., "Nuclear technology aspects of ITER vessel-mounted diagnostics", Journal of Nuclear Materials 417 (2011), 780-786
[8]S. Peruzzo, et al., "R&D on ITER in-vessel magnetic sensors", Fusion Engineering and Design 88 (2013) 1302 –1305
[9] O.N. Jarvis Plasma Phys. Control. Fusion **36** (1994) 209
[10] X. Zhang et al. Nucl. Fusion **54** (2014) 104008
[11] C. Hellesen et al. Plasma Phys. Control. Fusion **52** (2010) 085013
[12] J. Eriksson et al. Nucl. Fusion **55** (2015) 123026
[13] C. Cazzaniga et al. Rev. Sci. Instrum. **85** (2014) 043506
[14] M. Nocente et al. Rev. Sci. Instrum. **85** (2014) 11E108
[15] M. Tardocchi et al. Phys. Rev. Letters **107** (2011) 205002
[ ] M. Nocente et al. IEEE Trans. Nucl. Sci. 60 (2013) 1408
[16] M. Tardocchi, M. Nocente and G. Gorini Plasma Phys. Control. Fusion **55** (2013) 074014
[17] Maddaluno G et al. 40th EPS Conference on Plasma Physics P5. 102
[18] J Howard, 2015 JINST 10 P09023
[19] G. Gennacchi, A. Taroni, JETTO: a free boundary plasma transport code (basic version), Tech. rep., ENEA, RT/TIB 1988(5), Rome (Italy) (1988).
[20] G. Pereverzev, P. Yushmanov, ASTRA automated system for transport analysis in a tokamak, Tech. rep., Max-Planck-Institut fuer Plasmaphysik, Garching (Germany) (2002).
[21] D. Humphreys, et al., DIII-D Integrated plasma control solutions for ITER and next-generation tokamaks, Fus. Eng. Des. 83 (2–3) (2008) 193–197.
[22] G. De Tommasi, et al., XSC Tools: a software suite for tokamak plasma shape control design and validation, IEEE Trans. Plasma Sci. 35 (3) (2007) 709–723.
[23] T. Bellizio, et al., A MARTe based simulator for the JET Vertical Stabilization system, Fus. Eng. Des. 86 (2011) 1026–1029.
[24] S. Peruzzo, et al., Installation and commissioning of the JET-EP magnetic diagnostic system, Fus. Eng. Des. 84 (2009) 1495–1498.
[25] F. M. Callier, C. A. Desoer, Linear System Theory, Springer Verlag, 1991.
[26] R. Albanese, F. Villone, The linearized CREATE-L plasma response model for the control of current, position and shape in tokamaks, Nucl. Fus. 38 (5) (1998) 723–738.
[27] R. Albanese, R. Ambrosino, M. Mattei, CREATE-NL+: A robust control-oriented free boundary dynamic plasma equilibrium solver, Fus. Eng. Des. 96–97 (2015) 664–667.
[28] G. Marchiori, et al., Design and operation of the RFX-mod plasma shape control system, Fus. Eng. Des. 108 (2016) 81–91.
[29] R. Albanese, et al., Design, implementation and test of the XSC extreme shape controller in JET, Fus. Eng. Design 74 (1–4) (2005) 627–632.
[30] G. Calabrò, et al., EAST alternative magnetic configurations: modelling and first experiments, Nucl. Fus. 55 (8) (2015) 083005.
[31] A. Neto, et al., Conceptual architecture of the plant system controller for the magnetics diagnostic of the ITER tokamak, Fus. Eng. Des. 96–97 (2015) 887–890.
[32] R. Wenninger, et al., Advances in the physics basis for the European DEMO design, Nucl. Fus. 55 (6) (2015) 063003–7.
[33] M. Romanelli, et al., JINTRAC: A System of Codes for Integrated Simulation of Tokamak Scenarios, Plasma and Fus. Res. 9 (special issue 2) (2014) 3403023–1–4.
[34] G. Ambrosino, M. Ariola, G. De Tommasi, A. Pironti, Plasma Vertical Stabilization in the ITER Tokamak via Constrained Static Output Feedback, IEEE Trans. Contr. Sys. Tech. 19 (2) (2011) 376–381.
[35] M. Ariola, A. Pironti, The design of the eXtreme Shape Controller for the JET tokamak, IEEE Control Sys. Mag. 25 (5) (2005) 65–75.
[36] G. De Tommasi, et al., Shape control with the eXtreme Shape Controller during plasma current ramp-up and ramp-down at JET tokamak, J. Fusion Energ. 33 (2) (2014) 233–242.
[37] R. Albanese, et al., A MIMO architecture for integrated control of plasma shape and flux

expansion for the EAST tokamak, in: Proc. of the 2016 IEEE Multi-Conf. Syst. Contr., Buenos Aires, Argentina, 2016.
[38] G. De Tommasi, S. Galeani, A. Pironti, G. Varano, L. Zaccarian, Nonlinear dynamic allocator for optimal input/output performance trade-off: application to the JET Tokamak shape controller, Automatica 47 (5) (2011) 981–987.
[39] A. Lampasi, et al., The DTT device: power supplies and electrical distribution system, Fus. Eng. Des. This special issue.
[40] J. L. Terry et al., "Volume recombination and opacity in Alcator C-Mod divertor plasmas", Physics of Plasmas, 5, 1759-1766 (1998)
[41] V.A. Soukhanovskii et al., "Divertor heat flux reduction and detachment experiments in NSTX", Journal of Nuclear Materials, Volumes 363–365, 15 June 2007, Pages 432-436
[42] V.A. Soukhanovskii et al., "Divertor heat flux mitigation in the National Spherical Torus Experiment", Physics of Plasmas, 16, 022501 (2009)
[43] G. Hommen et al., "Real-time optical plasma boundary reconstruction for plasma position control at the TCV Tokamak", Nuclear Fusion, 54 (7), 073018 (2014)
[44] Hommen, Review of scientific instruments 11/2010; 81(11):113504
[45] J. F. Drake, "Radiative condensation in tokamak edge plasma", Physics of Fluids, 30, 2429-2433 (1987)
[46] E. Kolemen et al., "Heat flux management via advanced magnetic divertor configurations and divertor detachment", Journal of Nuclear Materials, 463, art. no. 48693, pp. 1186-1190 (2015)
[47] E. Lerche et al., "Optimization of ICRH for core impurity control in JET-ILW", Nuclear Fusion, 56 (3), art. no. 036022 (2016)

[48] A. Huber et al. , Journal of Nuclear Materials 363–365, 365 (2007), proc. 17th Int. Conf. on PlasmaSurface Interactions in Controlled Fusion Devices (PSI-17), Hefei, China, May 2006
[49] C. Grisolia et al. “Feedback control of highly radiative plasmas in Tore Supra”, J NUCL MAT, 275(1), pp. 95-100 (1999)
[50] J. P. Gunn et al. “Improvement of density control by feedback on Langmuir probe signals in Tore Supra ergodic divertor experiments”, Plasma Physics and Controlled Fusion, Volume 42, Number 5 (2000)
[51] L. Costanzo et al. “Detachment control by heat flux analysis on Tore Supra”, ECA Vol 25 A, 197 – 200 (2001)
[52] J. Neuhauser et al. “The Compatibility of High Confinement Times and Complete Divertor Detachment in ASDEX-Upgrade”, Plasma Physics and Controlled Fusion 37 (1995) A37 - A51
[53] H. Y. Guo et al. “Recent progress on divertor operations in EAST”, Journal of Nuclear Materials 415 (2011) S369–S374
[54] A. V. Chankin et al. “H-mode density limit and detachment in JT-60U”, Plasma Phys. Control. Fusion 44 (2002) A399–A405
[55] The JET Team (presented by R.D. Monk), “Recent Results from Divertor and SOL Studies at JET”, IAEA-CN-69/EX6/4, in Proc. 17th IAEA Fusion Energy Conference,Yokohama, Japan, 19-24 October 1998.
[56] Manduchi,G.;Fredian,T.;Stillerman,J "Future directions of MDSplus", Fusion Engineering and Design, 89(5), 780-783(2014)